ELSEVIER

Contents lists available at ScienceDirect

# **Extreme Mechanics Letters**

journal homepage: www.elsevier.com/locate/eml



# Dose-independent threshold illumination for non-invasive time-lapse fluorescence imaging of live cells



M.A. Bashar Emon <sup>a,1</sup>, Samantha Knoll <sup>a,1</sup>, Umnia Doha <sup>a</sup>, Lauren Ladehoff <sup>b</sup>, Luke Lalonde <sup>a</sup>, Danielle Baietto <sup>b</sup>, Mayandi Sivaguru <sup>c</sup>, Rohit Bhargava <sup>b,d</sup>, M. Taher A. Saif <sup>a,b,d,\*</sup>

- <sup>a</sup> Department of Mechanical Science and Engineering, University of Illinois at Urbana-Champaign, USA
- <sup>b</sup> Department of Bioengineering, University of Illinois at Urbana-Champaign, USA
- <sup>c</sup> Carle Woese Institute of Genomic Biology, University of Illinois at Urbana-Champaign, USA
- <sup>d</sup> Cancer Center at Illinois, University of Illinois at Urbana-Champaign, USA

#### ARTICLE INFO

Article history:
Received 7 February 2020
Received in revised form 19 February 2021
Accepted 21 February 2021
Available online 3 March 2021

Keywords:
Photo-relaxation
Illumination threshold
Non-invasive light
Time-lapse imaging
Traction force microscopy
Light intensity
Fluorescence microscopy

#### ABSTRACT

Fluorescent microscopy employs monochromatic light for excitation, which can adversely affect the cells being observed. We reported earlier that fibroblasts relax their contractile force in response to green light of typical intensity. Here we show that such effects are independent of extracellular matrix and cell lines. In addition, we establish a threshold intensity that elicits minimal or no adverse effect on cell contractility even for long-time exposure. This threshold intensity is wavelength dependent. We cultured fibroblasts on soft 2D elastic hydrogels embedded with fluorescent beads to trace substrate deformation and cell forces. The beads move toward cell center when cells contract, but they move away when cells relax. We use relaxation/contraction ratio ( $\lambda_r$ ), in addition to traction force, as measures of cell response to red (wavelength,  $\lambda$ =635-650 nm), green ( $\lambda$ =545-580 nm) and blue ( $\lambda$ =455-490 nm) lights with varying intensities. Our results suggest that intensities below 57, 31 and 3.5 W/m<sup>2</sup> for red, green and blue lights, respectively, do not perturb force homeostasis. To our knowledge, these intensities are the lowest reported safe thresholds, implying that cell traction is a highly sensitive readout of the effect of light on cells. Most importantly, we find these threshold intensities to be doseindependent; i.e., safe regardless of the energy dosage or time of exposure. Conversely, higher intensities result in widespread force-relaxation in cells with  $\lambda_r > 1$ . Furthermore, we present a photo-reaction based model that simulates photo-toxicity and predicts threshold intensity for different wavelengths within the visible spectra. In conclusion, we recommend employing illumination intensities below aforementioned wavelength-specific thresholds for time-lapse imaging of cells and tissues in order to avoid light-induced artifacts in experimental observations.

© 2021 Elsevier Ltd. All rights reserved.

#### 1. Introduction

Most living cells are photosensitive [1–3]. Furchgott and coworkers [4,5] showed that smooth muscles of mammalian arteries under tonic contraction relax their force on exposure to light. Recently, photorelaxation of fibroblasts was reported [6]. It is necessary to avoid such inadvertent effects; but it is still not clear how lights induce such responses in cells, as well as tissues. Since the advent of optical microscopy, various illumination techniques have been used to visualize cells and tissues. Recently however,

E-mail address: saif@illinois.edu (M.T.A. Saif).

URL: http://saif.mechse.illinois.edu/ (M.T.A. Saif).

monochromatic light is being used extensively for imaging. Many of these imaging methods involving fluorescent reporters and green fluorescent protein (GFP) require blue and green light excitation with wavelengths less than 550 nm where photosensitivity cannot be ruled out. This issue is particularly critical if the cells are exposed to high intensity light, repeatedly for time-lapse imaging. A number of imaging methodologies, such as optogenetics [7], super-resolution imaging [8,9], ion and voltage sensitive imaging [10], live cell imaging [3,9,11-13] may utilize hazardous levels of light [14]. A visible sign of photosensitivity or phototoxicity is the change in cells' morphology, such as blebbing, necrosis, formation of vacuoles, and mitochondrial swelling [2, 15]. Such morphological changes may be expressed at different phases of cell division [16,17] and may appear long after light exposure compared to the duration of exposure. In addition, it is possible to have effects associated to photo-toxicity that are not necessarily noticeable. Such external effects can compromise

<sup>\*</sup> Correspondence to: Micro and Nanotechnology Laboratory, University of Illinois at Urbana-Champaign, 2101D Mechanical Engineering Laboratory, 105 S. Mathews Avenue, Urbana, IL 61801, USA.

<sup>&</sup>lt;sup>1</sup> Authors contributed equally to the work.

data accuracy and experimental validity [18,19]. Hence, for live-cell imaging, it is imperative to eliminate the artifacts of light by choosing a suitable illumination protocol, which remained elusive for a long time.

Most of the previous studies on photo-toxicity relied on cellular reactions such as DNA damage [20] or apoptosis [13] due to high intensity lights. As instrumentation improves and imaging with lower incident intensities is possible, it becomes important to investigate the intensity and dose dependence as well. We choose contractility of cells as a read-out to quantify the effect of light, since force has been found to be correlated with a variety of functions such as cell migration [21], cellular homeostatsis [22], differentiation [23,24], morphogenesis, wound healing [25], disease progression and cancer metastasis [26-28]. Moreover, our previous works showed that fibroblasts relax their forces partially when exposed to toxic substances [29] or fluorescent lights commonly used in microscopes (wavelength,  $\lambda \sim 550$  nm and intensity,  $I \sim 2250 \text{ W/m}^2$ ) within 2 s of exposure [6,30]. We quantified the response by plating cells on soft Polyacrylamide (PA, 5 kPa) gel substrates functionalized with fibronectin and embedded with 100 nm fluorescent beads as fiduciary markers. The beads were placed within 1 µm from the surface of the gel substrate. Cells adhered to the substrates and generated contractile force. In response, the soft substrate deformed, and the beads followed the deformation, usually toward the center of the cell. The cell force reached a steady state within 3-4 h of plating after which the net force became nearly stationary with negligible fluctuations over a short span of time (minutes) [31,32]. After reaching this steady state, we exposed the cells with regular green light for either 2 s or 60 s, while we monitored the dynamics of the beads [6,30]. We found that soon after light exposure: (1) a majority of the beads moved away from the cell-center implying force relaxation, while a minority of beads moved toward cell-center implying contractility. This suggests a net force reduction, i.e., photorelaxation. (2) Some of the beads moved abruptly outward ("jumping"), implying sudden local force relaxation [33]. There is a need to relate these behaviors to experimental parameters such that potential experimental artifacts may be avoided.

Here, we systematically seek a threshold light intensity,  $I_{th}$  ( $\lambda$ ), below which cell traction becomes insensitive to light, i.e. the cells maintain force homeostasis without photo-relaxation, and yet the light is sufficient for high-resolution time-lapse fluorescence imaging. We performed our experiments by exposing fibroblasts (CV-1, CCD112CoN and NIH/3T3 cell lines) to red ( $\lambda = 635-650$  nm), green ( $\lambda = 545-580$  nm) and blue ( $\lambda = 455-$ 490 nm) lights with a range of intensities. The cells were plated on PA gel substrate functionalized with fibronectin and embedded with fluorescent beads. We measured the motion of beads for 1-8 hour(s) using a timelapse imaging approach. We quantified the relaxation/contraction ratio  $(\lambda_r)$  from the net bead displacement away from and toward the cell center.  $\lambda_r > 1$ implies that the cell has relaxed,  $\lambda_r = 1$  implies that the cell is maintaining force homeostasis. We found  $\lambda_r = 1$  for red lights with intensity of  $I = 57 \text{ W/m}^2$  or lower. Higher intensities and lower wavelengths resulted in  $\lambda_r > 1$ .  $I_{th}(\lambda)$  decreases with shorter wavelengths. We also quantified the net contractile force of the cells, which also remained unaffected by the lights with  $I < I_{th}(\lambda)$ . Above the threshold intensity, cell contractile force decreased with time. Furthermore, this threshold is not limited to cells on 2D substrates. We also verified that the threshold applies to multiple cell lines cultured on both fibronectin- and laminin-coated substrates.

#### 2. Materials and methods

#### 2.1. Cell culture

We used three types of cell lines for the study: normal monkey kidney fibroblast, CV-1 (ATCC), normal human colon fibroblast, CCD112CoN (ATCC), and mouse embryonic fibroblast, NIH 3T3 (ATCC). The effect of light was studied for both 2D and 3D culture. CV-1 and CCD112CoN were cultured on 2D substrates, 3T3 were cultured in 3D. Cells were cultured in fibroblast media containing 89% Dulbecco's modified Eagle's medium (DMEM) (Corning), 10% fetal bovine serum (FBS) (Gibco) and 1% penicillin-streptomycin (Lonza). During imaging, cell culture media without phenol red was used.

#### 2.2. Polyacrylamide 2D substrate preparation

CV-1 cells were plated on Polyacrylamide (PA) hydrogels embedded with fluorescent particles. The beads were localized at a depth of about 1  $\mu$ m from the top surface of the substrate following a protocol outlined in [34]. We used three types of fluorescent beads - (i) 0.2 \(\mu\)m-dia dark red beads (excitation/emission-660/680 nm, Thermo-Fisher, cat. no. F8807) (ii) 0.1 µm red beads (excitation/emission-580/605 nm, Thermo-Fisher, cat. no. F8801) and (iii) 0.2 µm yellow-green beads (excitation/emission-505/515 nm, Thermo-Fisher, cat. no. F8811) The bead colloidal solution was diluted to a concentration of about 7 imes 10  $^9$  particles/ml in order to maintain a bead density of approximately 1 per 5  $\mu$ m<sup>2</sup> on the gel surface. The elastic modulus of the hydrogels was approx. 5 kPa (4.47  $\pm$  1.19) based on the protocol established by Tse and Engler [35]. 5% Acrylamide and 0.15% Bis-acrylamide concentration was achieved by mixing 1.25 ml 40% Acrylamide (Sigma-Aldrich) stock solution, 0.75 ml 2% Bis-acrylamide solution (Sigma-Aldrich) and 8 ml DI water. Polymerization was initiated with 1% Ammonium persulfate (APS. Bio-Rad) and 0.1% Tetramethylethylenediamine (TEMED, Bio-Rad) in final concentration. After polymerization, the PA gel substrates have an approximate depth of 110 µm.

After polymerization, substrates were functionalized with two types of ECM, namely fibronectin (Human, Corning) and laminin (Human, Corning). Two ECMs were chosen to eliminate the possibility that photo-relaxation might be an artifact of a particular ECM. The protocol for functionalization is outlined by Tse and Engler [31]. Briefly, 0.2 mg/ml sufosuccinimidyl-6-(4'-azido-2'-nitrophenylamino)-hexanoate (Sulfo-SANPAH, Thermo Scientific) solution in HEPES buffer (50 mM HEPES at pH 8.5, Fisher Scientific) was applied to the PA gels and then was activated with 365 nm UV light (8 Watt, UVP UVL-28, Analytik Jena, US). The substrates were then immersed overnight in fibronectin or laminin solution in HEPES buffer. Concentration of 25  $\mu$ g/ml was used for both fibronectin and laminin. The gels were then washed with PBS and were ready for cell culture. CCD112CoN (ATCC) cells were tested on 2D PA gel substrate following the above protocol. However, only fibronectin functionalization was tested with these

# 2.3. 3D Collagen scaffold preparation

Collagen precursor solution was prepared on ice by first neutralizing rat-tail collagen I (Corning) with 1N sodium hydroxide, 10X PBS, and deionized (DI) water. We followed Corning recommended protocol [36] to prepare a final collagen solution of 2.5 mg/ml with pH 7.2 from a high concentration stock solution of 8.9 mg/ml in 0.02 N acetic acid (280.9  $\mu$ l collagen stock sol., 6.5  $\mu$ l NaOH, 100  $\mu$ l 10X PBS and 612.6  $\mu$ l DI water). NIH/3T3 (ATCC) cells were then mixed with collagen at a density of 0.1 million/ml.

This mixture was dispensed in a glass-bottom petri-dish (well diameter 12 mm, depth 1 mm, Cellvis). After filling the well with cell-collagen mixture, the well was covered with coverslip (22 mm, EMS). The petri-dish was then flipped and immediately put in the refrigerator at 4 °C so that the cells settle down to the cover slip while the collagen does not completely polymerize. After 15 min, samples were flipped again and kept in the incubator (37 °C) for 3 min which allowed the cells to fall under gravity through the liquid collagen while it polymerizes simultaneously. The petri-dish was flipped 2 more times and the time intervals between the flips were 5 and 7 min respectively in the incubator. The cover slip was removed and the dish was filled with cellculture media. From z-stack images, sample thickness was found to be 900 µm, and cells were observed in different planes. We selected a plane 500 µm above the bottom of the dish to ensure that cells were completely surrounded by 3D collagen matrix.

#### 2.4. Light source and illumination methods

The cells were illuminated continuously with either: (1) a deep red collimated LED (light emitting diode) (Thorlabs, Inc., Newton, NJ) coupled with far red filter set (Semrock Brightline LF635/L P-B-000, Rochester, NY) giving  $\lambda = 635-650$  nm considering full width at half maximum (HMFW) intensity or (2) a fluorescent metal halide lamp (X-Cite® Series 120, Excelitas Technologies, Waltham, MA) coupled with an mCherry filter (Semrock Brightline mCherr y - M - O MF, Rochester, NY) giving  $\lambda = 545-580$ (HMFW) or a GFP filter set (Semrock Brightline GFP-3035C-000, Rochester, NY) giving  $\lambda = 455-490$  (HMFW). These range of wavelengths were measured by spectral analysis of the illumination using a standard spectrometer (USB2000+, OceanOptics) (Suppl. Fig. 1. Technical details about the light sources and the filters are provided in Supplementary Information. Suppl. Fig. 2 shows a schematic diagram of the experimental setup and light paths. Neutral density (ND) filters were employed for both sources to tune light intensity. For example, ND100 and ND25 indicate 100% and 25% of the light were transmitted. In addition to ND filter, power output from the fluorescent metal halide lamp for mCherry light was modulated to control light intensity. Thus, 25%ND25 means that 25% of light was allowed from the source, and 25% of this output was filtered by the ND25 filter. The intensity of LED light was controlled by the ND filters only. The light sources and their intensities are shown in Table 1. Light intensities were measured using 40X water immersion objective (Numerical Aperture, NA = 1.15, Olympus) by PM100 power meter (ThorLabs) at a plane 15.5 mm above the objective and at the focal plane which is the typical location of the sample. Note that the power meter aperture is large (9.5 mm) and could not be used to quantify the special intensity profile of the incident light. In order to reduce the aperture, the sensor was wrapped with an aluminum foil with 0.75 mm diameter aperture. Thus, the intensity was measured for light passing through the small aperture only. The power meter was moved orthogonal to the incident light and along the radial direction of the light beam to measure the spatial intensity profile. Also, it was not possible to measure light intensity at the sample planes during experiments due to the presence of cells. Hence intensity was measured at a distance of 15.5 mm above the objective. Although, the intensity can then be estimated at the focal plane (sample plane) from the measurements at the 15.5 mm plane, we measured the intensity at the focal plane as well in the absence of cells to ensure minimal loss of light due to dispersion. The correlation between the measured intensities at the two planes was used to estimate light intensity on cells. Intensity profiles of representative light sources are provided in Suppl. Fig. 3.

**Table 1** Illumination intensities and corresponding particle tracking precision for various light sources.

Lighting condition	Avg. intensity at 15.5 mm from the objective (W/m²)	Max. intensity at cell sample plane $(W/m^2)^b$	
LED ND6	0.12	14.6	18.07
LED ND12	0.28	34.1	14.84
LED ND25	0.47	57.2	10.62
LED ND100	1.93	234.8	6.1
mCherry 12% ND6	1.43	257.7	13.11
mCherry 25% ND6	2.47	445.0	9.77
mCherry 12% ND12	3.17	571.1	9.05
mCherry 25% ND12	5.53	996.4	7.57
mCherry 25% ND25	12.5	2252.2	11.24
mCherry 25% ND100	40.8	7351.1	6.71
mCherry 100% ND25	41.65 <sup>a</sup>	7504.2	-
mCherry 100% ND100	135.94 <sup>a</sup>	24493.7	-

Displacement distributions for cells exposed to various light sources, listed in order of increasing light intensity. Particle tracking precision determined by tracking beads immobilized in PA gels devoid of cells during one-minute of continuous illumination through 40X water immersion objective (NA=1.15). Illumination source column indicates light source (LED or mCherry), as well as the accompanying neutral density (ND) filter classification. ND100 indicates no filter was used (i.e. 100% of light passed through). Modulation of relative power output for the fluorescent metal halide lamp utilized as the mCherry source is indicated, preceding the ND classification (i.e. 12 or 25%). Tracking precision computed as standard deviation of the Gauss fit of the displacement distribution for each illumination source. Each illumination source represents over 1000 particles from 3 distinct gel substrates.

<sup>a</sup>Values reported was determined from extrapolation of experimental data.

#### 2.5. Particle tracking and limitations

Inspected cells on 2D substrates were more than 100 µm away from neighboring cells. The motion of fluorescent beads was tracked from images for analyzing their movements with time. First, the cell spreading area was determined and the centroid of the area was established using the formula: centroid  $(\bar{x}, \bar{y}) = (\frac{\int x dA}{\int dA}, \frac{\int y dA}{\int dA})$ ). Here, cell boundary gives the limits of the integrals. Let the vector from the origin (cell centroid) to an embedded fluorescent bead be r(0) and r(t) at time = 0 and time = t respectively. Hence, the net magnitude and direction of displacement of the bead is given by |r(t)|-|r(0)|. Motions of all the beads within cell area were computed and statistically analyzed for cells subjected to the described illumination protocols. Motion toward the centroid (inward) is negative and represents cell contraction; motion away from the centroid (outward) is positive and represents cell relaxation. Relaxation was assessed by a majority of motion outward relative to inward. It is expected that cells exposed to sufficiently low intensity light would not exhibit light-induced relaxation. However, lowering the excitation light intensity reduces the signal level with respect to background noise, thus reducing the particle tracking precision. We quantified the noise and measurement resolution for each light source (see Table 1) by tracking fluorescent beads in PA gels without adherent cells. For each illumination condition, light was shined for 60 s. Bead displacement was quantified as the change of position with an arbitrary origin during 60 s, i.e., |r(60)||r(0)|. A Gaussian curve was fit to probability distributions of the

<sup>&</sup>lt;sup>b</sup>Sample plane intensity was determined employing intensity profiles in suppl. Fig. 3.

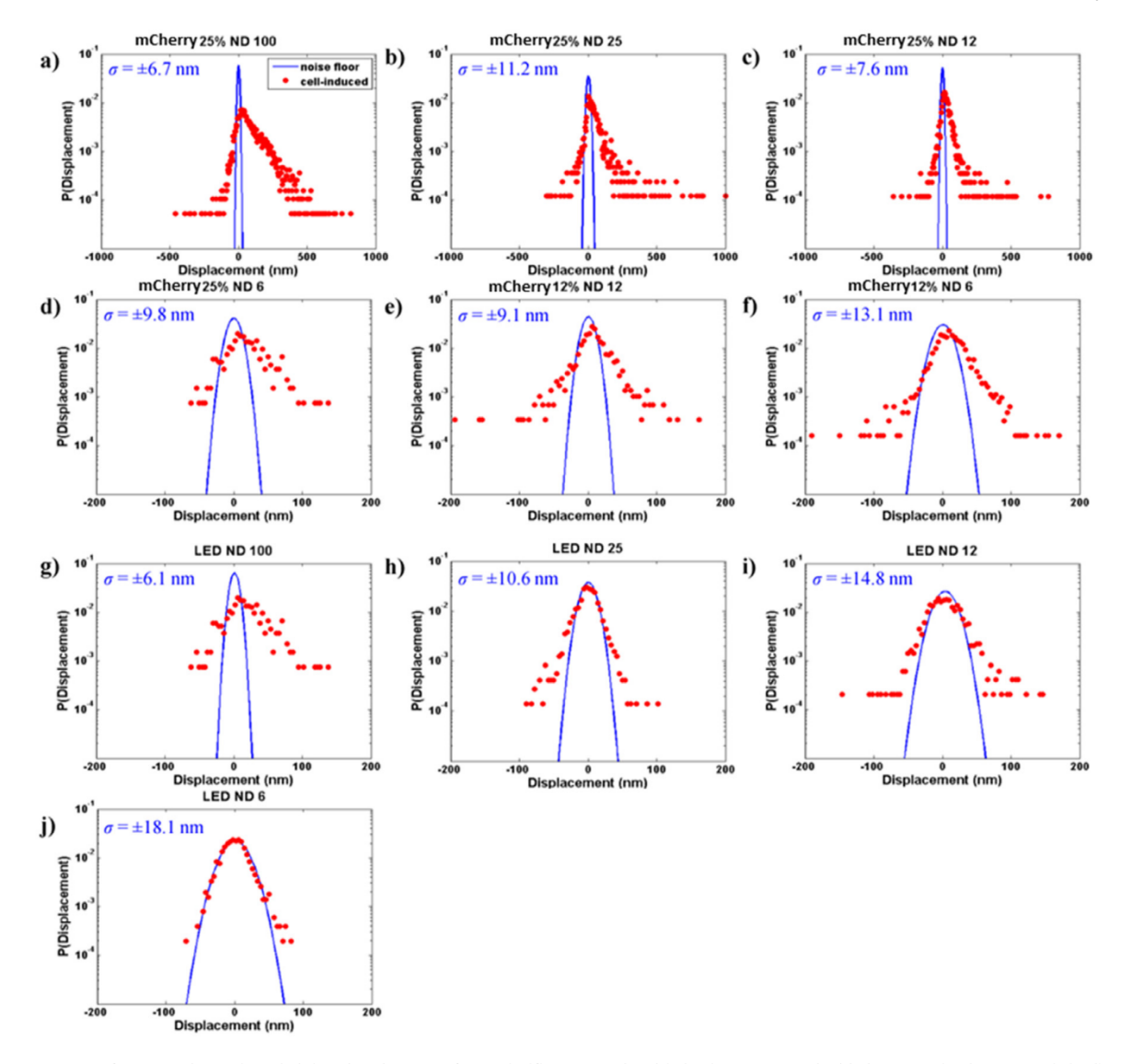


Fig. 1. Determination of noise and signal. Probability distributions of particle (fluorescent beads) displacements embedded in PA gel substrate with (red) and without (blue) CV-1 cells ( $n \ge 10$ ) for various illumination conditions (a–j). For each case, light exposure time was 60 s. Particle displacement is quantified as the change of position after 60 s, i.e., |r(60)| - |r(0)|, where r(t) is the vector location of the particle. Tracking precision is estimated as the standard deviation of Gauss fit of the displacement distribution for the cell-free substrates. Each illumination source represents over 1000 beads from 3 distinct gel substrates. The variances of the distributions were determined according to an F-test ( $\alpha = 0.05$ ). (For interpretation of the references to color in this figure legend, the reader is referred to the web version of this article.)

particle motion. The standard deviation  $(\sigma)$  of the distribution represents a measure of displacement resolution for each light source (Table 1, Fig. 1). For evaluation of cell response, sparsely populated fibroblasts were then cultured on the same substrates with beads. Single cells were exposed to various illuminations (Fig. 1) for prescribed durations. The displacements of beads within the footprint of each cell were then analyzed and reported. The probabilities of contraction,  $(P_c)$  and relaxation  $(P_r)$  were evaluated by integrating the area under the left and the right sides of probability distributions (red points) in Fig. 1 for each illumination condition. Relaxation ratio was determined as,  $\lambda_r = P_r/Pc$ .

Monitoring cell traction over a long period after target light exposure requires excitation of the tracer beads embedded in the substrate. In order to minimize the effect of observation light on cells, we use dark red beads that can be traced with low intensity light (long wavelength LED, ex/em-660/680 nm with I < 57 W/m²) with minimal dosage. However, most of the experiments are not constrained by this limitation. For example, cells exposed to 60 or 120 s mCherry light was monitored using 0.1 µm red beads

(ex/em-580/605 nm) that do not require a different observation light. Similarly, for monitoring cells that were exposed to continuous LED light, we used dark red beads (ex/em-660/680 nm) that have the same excitation light. Nevertheless, when beads are monitored after cells are exposed to prescribed target dosage of light, the monitoring illumination with sub-threshold light may still affect cell traction. To assess the impact of such observation light, we carried out an extensive dosage analysis for various illumination conditions (Table S1). The analysis reveals that for most of the cell exposure conditions, initial target dosage on cells for 60 s or 120 s is more than 96% of the total illumination which indicates that the effect of light for monitoring is minimal.

#### 2.6. Application of various light dosages

In order to determine a safe illumination on cells, at first we considered reducing the radiation intensity and then reducing the amount of exposure time at a given intensity. It should be noted that adherent, non-motile cells maintain a steady contractile state, or force homeostasis after a few hours of plating [15,

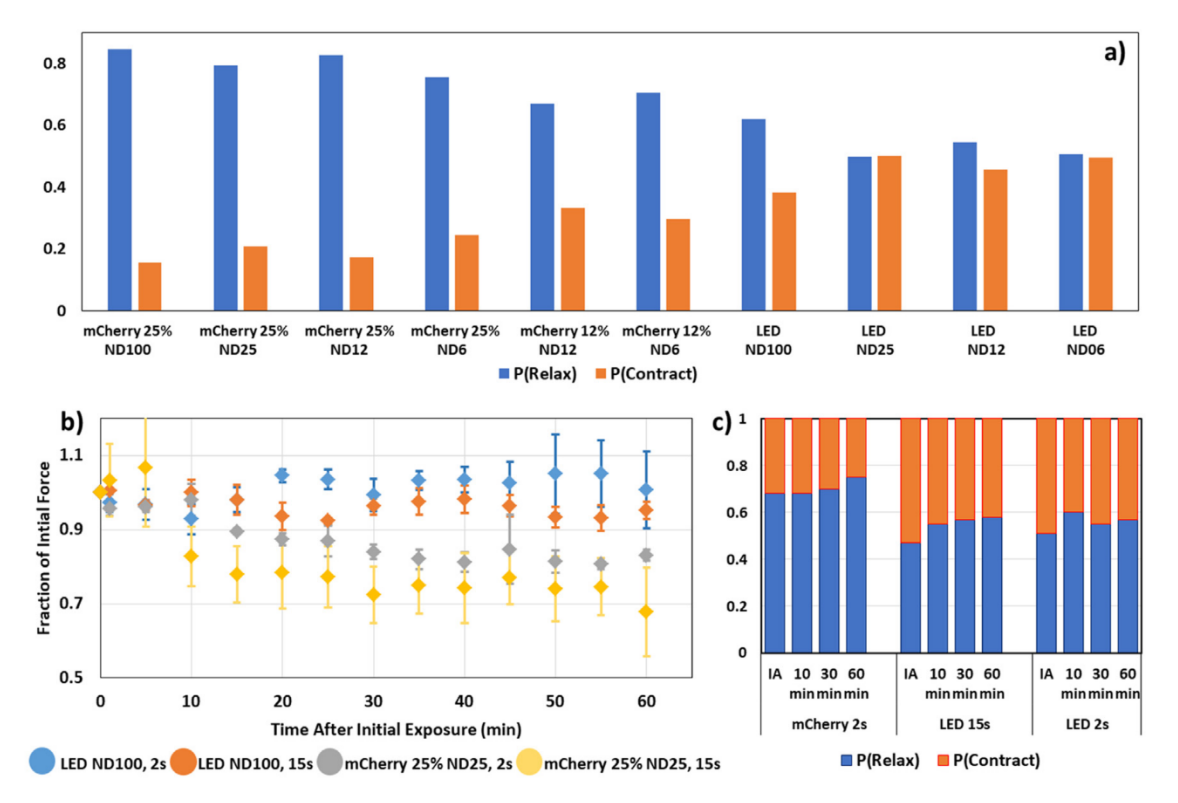


**Fig. 2.** Cellular force relaxation strongly correlates with light intensity. (a) Cell force relaxation decreases with decreasing light intensity during illumination. Proportion of outward – relative to inward – moving beads represents decreasing dominance of force relaxation over contraction throughout illumination. Probability (P(Relax)) of outward-moving bead displacements relative to the cell centroid decreases with decreasing illumination intensity (blue columns). On the other hand, probability of inward motion, P(Contract) = 1-P(Relax), increases with decreasing intensity (orange columns). All cells were illuminated continuously for 60 s. Each illumination condition represents n = 5 distinct cells. (b) Time evolution of traction force following illumination for various exposure conditions. Traction forces over time as a fraction of initial force for cells exposed to the following illumination sources: LED (Dark red light) ND100 for t = 2 s (blue), LED (Dark red light) ND100 for t = 2 s (orange), mCherry 25% (Green light) ND25 for t = 2 s (gray), or mCherry 25% (Green light) ND25 for t = 15 s (yellow). Time t = 0 represents the force at the instant the illumination period started. Each distribution represents an average for t = 3 cells. Error bars represent standard error of the mean (SEM). (c) Probability of relaxation (P(Relax)) and contraction (P(Contract)) evaluated by integrating the area under the left and the right sides of probability distributions (red points) in Fig. 1 for each illumination condition (mCherry 25% ND100, t = 2 s; LED ND100, t = 2 s). Force relaxation shown at 0 s (Immediately after, IA), 10 min, 30 min, 60 min after illumination, all normalized with the force at 0 s. Each column represents an average of t = 3 cells and number of beads >1000. Number of independent experiments: 3. (For interpretation of the references to color in this figure legend, the reader is referred to the web version of this article.)

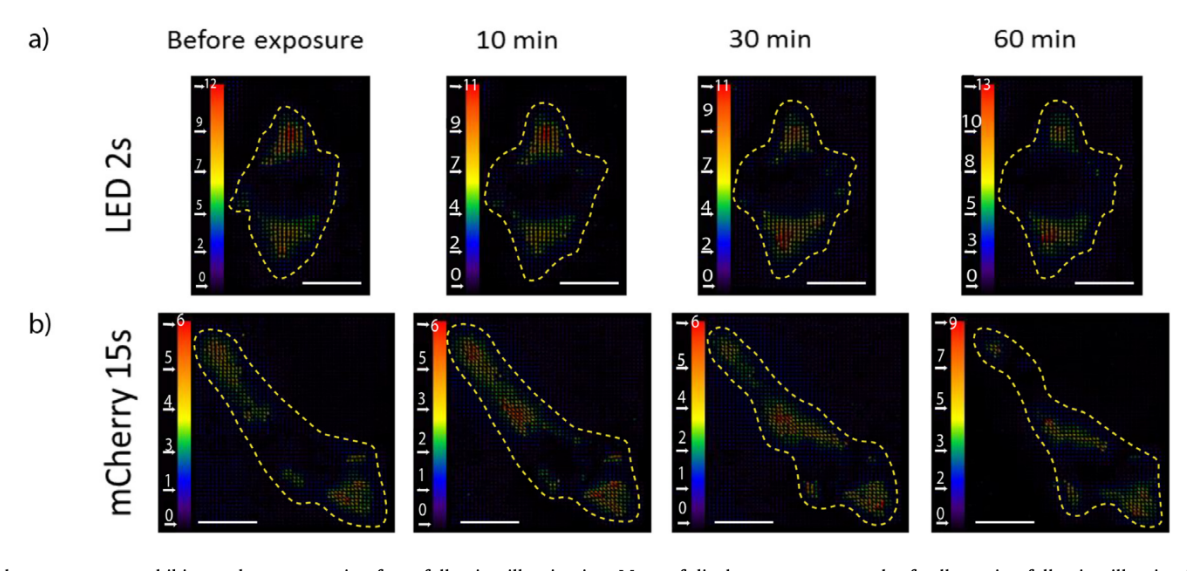


**Fig. 3.** Displacement maps exhibit steady state traction force following illumination. Maps of displacement as a result of cell traction following illumination by either (a) LED ND100 for t = 2 s or (b) mCherry 25% ND100 for t = 15 s. Unit bar in pixels (1 pixel = 0.167 um). Scale bar: 20 um.

31,37–40]. The goal was to search for the light (wavelength and intensity) that allows cells to maintain force homeostasis. To this end, we exposed CV-1 cells, plated on PA gels functionalized with

fibronectin and laminin independently, to continuous illumination for 60 s with various lighting sources. Substrate deformations were assessed as "contractile" when the beads moved toward the cell center, or "relaxation" when the beads moved outward [34]. These experiments provided with initial evidence of a threshold intensity of light that does not perturb cell traction homeostasis.

To investigate the effect of energy dosage, we exposed the cells to green and red lights for 15 s and 2 s and measured relaxation for the following hour. Cell contraction or relaxation was measured using the LED light source ( $\lambda = 635-650$  nm with  $I < 57 \text{ W/m}^2$ ), which was found to be non-invasive from previous results. We also ensured that the dosage required for observation was negligible compared to the target illumination dosage (see Table S1). Intriguingly, results from these experiments led us to a hypothesis that the threshold intensity is dose-independent, i.e. light with intensities below the threshold limit are noninvasive irrespective of the exposure time or energy input to the cells. To further test this hypothesis, we carried out two sets of experiments with intensities below threshold, for extremely long exposures – (i)  $\sim$ 200–1600 ms every 5 min for  $\sim$ 8 h total duration (ii) 60 min continuous irradiation (dosage details in Table S1). Findings from the experiments are presented in the following sections.

#### 3. Results

#### 3.1. Lower wavelength light causes more photo-relaxation

Probability distributions (normalized histograms such that the area under the histogram equals to 1) of displacements induced by CV-1 cells exposed to each light source are shown in Fig. 1aj (red points). Gauss-fit of the noise floor is superimposed on the histograms (blue lines in Fig. 1a-j, merged plot shown in Suppl. Fig. 4). Deviation of the cell-induced motion (red) from the noise-floor (blue) indicates the extent to which active cell motion occurs beyond the measurement noise. The variances of the distributions were determined according to an F-test ( $\alpha =$ 0.05). A positive skewness indicates relaxation whereas a negative skewness means contraction. Substrate deformations of all mCherry-exposed CV-1 cells exhibit significant statistical deviation from the noise-floor (Fig. 1a-f). This also holds true for cells exposed to the LED ND100 source (Fig. 1g). However, for LED ND6, a large portion of the cell-induced motion aligns with the noise floor (Fig. 1j). Thus, very little activity is detected beyond the measurement noise for LED ND6 source. This can be due to the fact that the cells do not produce any excess force on the substrate during this 60 s period. For LED ND25 and ND12, cell induced motions are detected beyond noise floor, and the distributions are symmetric, i.e., the cells' contractility and relaxation during 60 s time are balanced, resulting in force homeostasis. While cells can maintain force homeostasis under exposure to any of the sources (LED ND25, LED ND12, LED ND6), we identify LED ND25 as a threshold light source that offers a compromise between minimal photo-relaxation and sufficient brightness for time-lapse imaging of cells and substrate beads.

The probabilities of relaxation compared to contraction increases with higher intensities and smaller wavelengths of light (Fig. 2a). This suggests that wavelength may also play an intrinsic role, as longer wavelength sources are known to reduce damage to cells [13]. Cells exposed to red light with intensity below 57 W/m², for example, exhibit equal proportions of contraction and relaxation with  $\lambda_r \sim 1.0$  (Fig. 2a). This shows evidence of a limit intensity that is safe for the cells.

# 3.2. Time evolution of traction forces suggests that cells maintain a steady state following initial illumination period

Traction forces of living cells have traditionally been thought to attain a steady state soon after ( $\sim$ 2 h) adhering to a surface [15, 31,37–40]. Under normal circumstances, this force homeostasis

is maintained until initiation of other activities, e.g., migration or division. In this study, we aimed to understand how traction forces evolve over time following illumination with potentially damaging lighting conditions. For investigating traction evolution, we varied intensity, as well as exposure times and thus input dosages. Four different lighting conditions were utilized: mCherry 25% ND100 for (i) t=15 s and (ii) t = 2 s, and LED ND100 for (iii) t = 15 s and (iv) t = 2 s. The LED ND25 was chosen as the non-damaging light source for traction monitoring (based on Table 1 and Fig. 1). Cell traction was monitored for 60 min after light exposure. As expected, the greatest decrease in traction force occurs for the mCherry 25% ND100 for t = 15s condition, followed by mCherry 25% ND100 for t = 2 s, LED ND100 for t = 15 s followed by LED ND100 for t = 2 s (Fig. 2b). In all cases, traction forces decrease initially within first 15 min. After initial decline, force values for each light condition maintain a steady-state, fluctuating within  $\pm 5\%$ , for subsequent  $\sim 45$  min. Hence, these results suggest two key points - (a) force relaxation decreases with decreasing light intensity, and (b) for the same intensity, higher energy dosage (i.e. longer duration of exposure) causes higher relaxation.

A measure of the change in contraction-relaxation is given by the probabilities of bead displacements inward (contraction),  $P_c$ , and outward (relaxation),  $P_r$ , of the cell center respectively. These probabilities are shown in Fig. 2c for cells exposed to mCherry 25% ND25 for t=2 s, LED ND100 for t=15 s and 2 s. Soon after exposure to mCherry 25% ND25 for t=2 s,  $\lambda_r=P_r/Pc\sim$ 2.1. This ratio increases to  $\sim$ 3.0 after 60 min, while net force decreased by 20% during this time (Fig. 2b).  $\lambda_r$  is close to 1.0 soon after both exposures to LED ND100 light. However, higher dose with 15 s exposure resulted in a steady relaxation; whereas the lower dose caused initial relaxation that was followed by contractile recovery. Force evolution curves (Fig. 2b) indicate similar trends. Hence, these results underscore the fact that changes in  $\lambda_r$  strongly correlate with changes in cell force, and hence is a reasonable index for monitoring traction behavior.

It is important to note that bead relaxation probability or traction relaxation provides a cumulative response from all locations underneath the cell spreading area. However, cells can interact with the substrate with considerable spatial heterogeneity. As a result, even though cells maintain  $\lambda_r$  over time, inspection of the individual bead displacements from local traction forces shows evidence of small, localized force changes. Cell-induced displacement maps reveal spatio-temporal modulation of traction throughout the spreading area of the cell (Fig. 3). While the location of the largest displacements shifts throughout the one-hour observation period, the dominant angle/orientation along which the forces are aligned appears to remain constant.

## 3.3. Photo-relaxation is not specific to ECM, cell line or 2D culture

In order to test whether the observed photo-relaxation is an artifact of fibronectin ECM, we plated CV-1 cells on PA gel substrates functionalized with laminin. We exposed the cells to the following lighting conditions: (i) mCherry 100% ND25 (I =  $7500 \text{ W/m}^2$ ) and (ii) mCherry 100% ND100 (I =  $24,500 \text{ W/m}^2$ ), each for 120 s. For both light conditions, the beads were imaged every 5 s for a total of 2 min. Probability distribution of bead displacements after 2 min with mCherry lights are presented in Suppl. Fig. 5a–b. The distributions are positively skewed which indicate force relaxation due to both illuminations. Also, as expected, the distribution was relatively more skewed for mCherry 100% ND100 due to higher intensity. Corresponding bead displacements for representative cells after a 120 s illumination period is shown in Suppl. Fig. 6A–B. It is clear that force relaxation is significantly more pronounced as

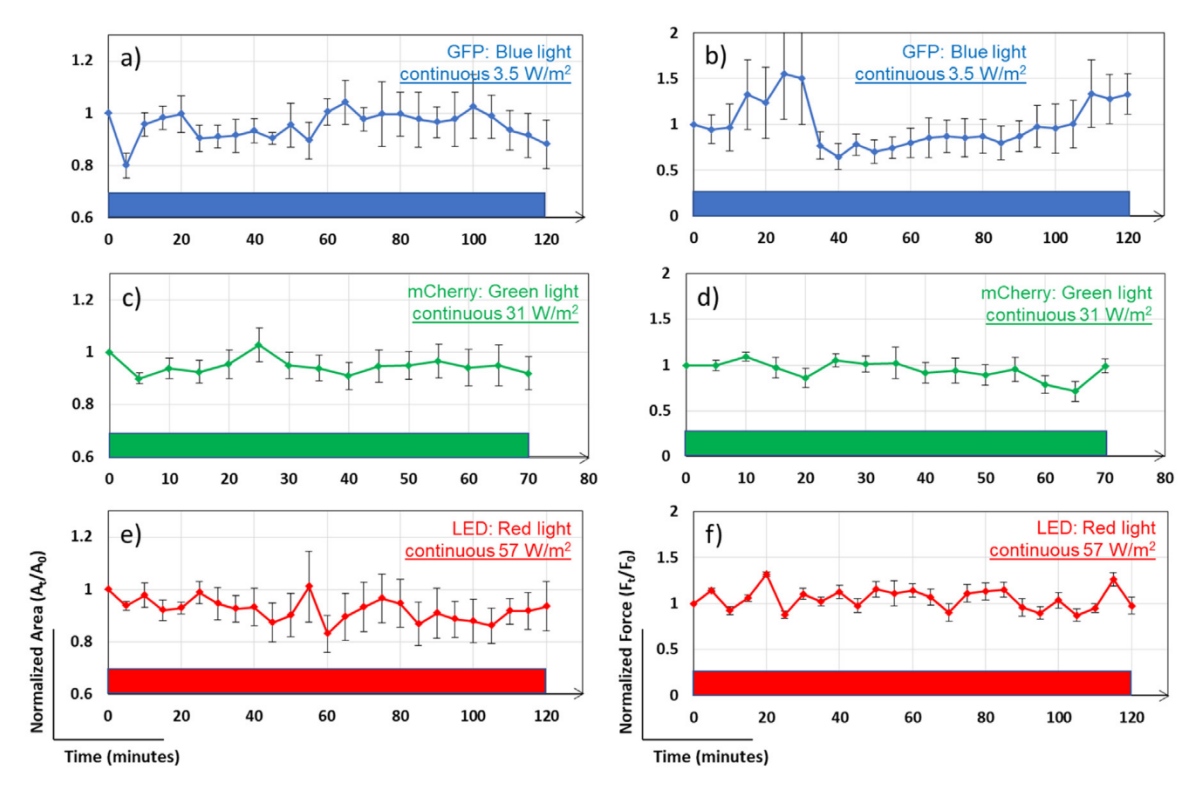


**Fig. 4.** Threshold illumination intensity is dose-independent for extremely long continuous exposure. CV-1 fibroblasts were subjected to (a-b) GFP (n = 5), (c-d) mCherry (n = 11) and (e-f) LED (n = 3) lights at threshold light intensity for at least 60 min. Images were captured every 5 min to analyze cell spreading area (a, c, e) and total cell force (b, d, f). The parameters were normalized with respect to initial values (at t = 0 min). All spreading area and force curves for these illuminations stay close to unity, which indicates undisturbed force homeostatsis and hence, no effect of light on cell traction and relevant functions. Number of independent experiments: 3. Error bars represent SEM.

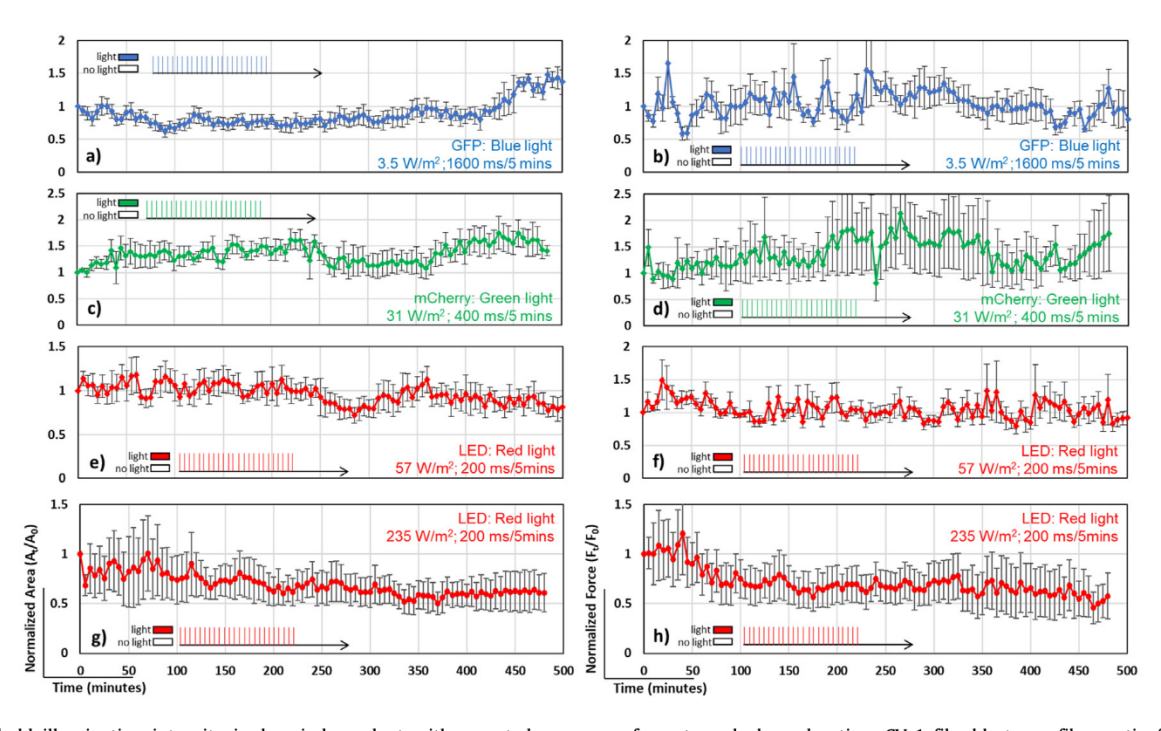


Fig. 5. Threshold illumination intensity is dose-independent with repeated exposures for extremely long duration. CV-1 fibroblasts on fibronectin functionalized substrates, were subjected to (a-b) GFP (n = 6), (c-d) mCherry (n = 5) and (e-f) LED (n = 5) lights pulses at threshold light intensities for  $\sim$  24 h. Images were captured every 5 min to analyze cell spreading area (a, c, e) and total cell force (b, d, f). Pulse durations for GFP, mCherry and LED lights were 1600, 400 and 200 ms respectively. Normalized spreading area and force curves for all the illuminations stay close to unity, which indicates that repeated exposure to light below threshold intensity does not perturb force homeostatsis; even with experiments that have very long durations. (g-h) Normalized cell area and total force curves for LED red light with intensity higher than threshold (I = 235 W/m²) show steady reduction in spreading area and relaxation of traction force. Within  $\sim$  8 h, these parameters dropped to almost half of the initial values. These results ascertain that traction force is a reliable indicator of photo-toxicity and our established threshold intensities do not induce unwarranted photo-response in cells. Number of independent experiments: 4. Error bars represent SEM.

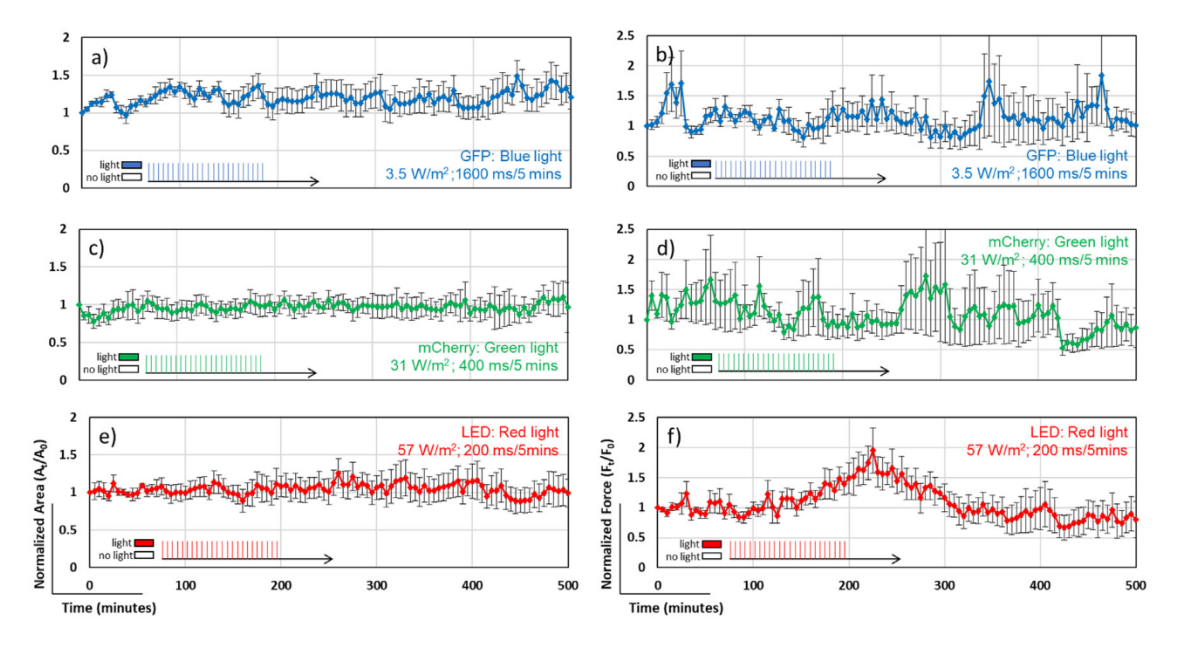


Fig. 6. Dose-independent threshold intensity is applicable for laminin ECM functionalization. CV-1 fibroblasts on laminin coated substrates, were subjected to (a-b) GFP (n = 6), c-d) mCherry (n = 6) and (e-f) LED (n = 5) lights at threshold light intensity for  $\sim$  24 h. Images were captured every 5 min to analyze cell spreading area (a, c, e) and total cell force (b, d, f). Exposure times for GFP, mCherry and LED lights were 1600, 400 and 200 ms respectively. Similar to results with fibronectin in Fig. 5, normalized spreading area and force curves for all the illuminations stay close to unity. This suggests that light below threshold intensity does not perturb force homeostatsis irrespective of adhesion ECM, even with repeated exposure for long duration. Number of independent experiments: 3. Error bars represent SEM.

compared to contraction, which is similar to the results with fibronectin. These results suggest that photo-relaxation is not specific to fibronectin-rich ECM.

We anticipated that photo-relaxation is not limited to CV-1 cell line. Hence, we explored the effect of light on human (CCD-112 CoN, colon normal fibroblast) and mouse cells (NIH/3T3 fibroblasts) as well, the latter in 3D discussed below. We performed traction force microscopy on CCD112CoN cells during and after 120 s exposure to (i) LED ND25, (ii) mCherry 100% ND25 and (iii) mCherry 100% ND100. The results are presented in Suppl. Fig. 5c. As expected, both mCherry lights induced force relaxation throughout the entire 120 s of illumination. During the following hour, these cells maintained a steady state as observed with CV-1 cells as well. On the other hand, the LED light source, which illuminated at an intensity level below the anticipated threshold, triggered no such relaxation. Hence, we can deduce that human fibroblasts are also susceptible to photo-relaxation if irradiated with above-threshold light. However, the precise threshold light for CCD112CoN may differ from that for CV-1 cells.

The above studies were limited to cells cultured on 2D substrates. To investigate the effect of light on cells in 3D extracellular matrix, we cultured NIH/3T3 fibroblasts in collagen matrix. After 1 hr of polymerization of the cell-ECM mixture, the cells were exposed to (i) mCherry 100% ND25 (ii) LED ND25 illuminations for 120 s Following the exposure, we observed the cells for the next 10 h using only phase-contrast imaging. The cells not exposed to light (mCherry or LED) probed the microenvironment using filopodia to elongate and migrate (Suppl. Vid. 1, n = 10 cells). In stark contrast, cells exposed to mCherry 100% ND25 illumination underwent slowing down of activity followed by severe blebbing (Suppl. Vid. 2, n = 10 cells) and apparent death. However, cells exposed to LED ND25 illumination appeared to be similar to control cells (not exposed to light), i.e., they were elongated, contractile and migratory (Suppl. Vid. 3, n = 10 cells). Hence, these results suggest that the threshold intensity of 57 W/m<sup>2</sup> is possibly valid for NIH/3T3 fibroblasts within 3D collagen matrices as well.

3.4. Threshold intensity of monochromatic light is dose-independent, but wavelength-specific

Our results suggest that 57 W/m<sup>2</sup> is a threshold intensity for red light with wavelengths longer than 650 nm. The next question we set out to explore is whether this safety limit applies to shorter wavelengths. To this end, we expanded our investigation to green and blue lights since these are widely used in fluorescence microscopy. As anticipated, the shorter wavelengths have lower thresholds. We found that the safe intensities for green (mCherry,  $\lambda = 545-580$ ) and blue (GFP,  $\lambda = 455-490$ ) lights are 31 and 3.5 W/m<sup>2</sup> respectively. These thresholds for green and blue light were determined by trial-and-error experiments with short durations. We reduced intensity from 57 W/m<sup>2</sup> and performed preliminary experiments for short exposures (60 s). If 60 s exposure showed no relaxation, we then carried out experiments with 60 min continuous exposure. If 60 min exposure was safe, we carried out the pulsed exposure experiment for  $\sim$ 8 h. These results suggest that mechanisms that induce photo-toxicity are intrinsically wavelength-dependent.

Next, we investigated whether the threshold intensity is doseindependent i.e. safe regardless of the energy dosage. To test this, we exposed the cells to threshold intensities for long duration that produces a very high energy input. Two modes of illumination were tested — (i) continuous exposure for more than 60 min (Fig. 4), and (ii) pulse exposure (pulse duration, 200–1600 ms, Fig. 5) every 5 min for  $\sim$ 8 h. Both conditions transmitted high total dosages (Table S1). Remarkably, despite being exposed to such high energy irradiation, the cells showed no signs of distress or toxicity with regards to cell traction. Fig. 4 shows that cell spreading area and total traction force remains unaffected during continuous exposure to threshold intensities for 60-120 min. Fig. 5 presents data that establishes safety of intensities below reported thresholds with repeated exposures for long durations. Suppl. Fig. 7 shows cell spreading area for control cells that were not illuminated with fluorescent lights. As expected, evolution of cell area for control cells is similar to those of cells exposed to fluorescent intensities below threshold.

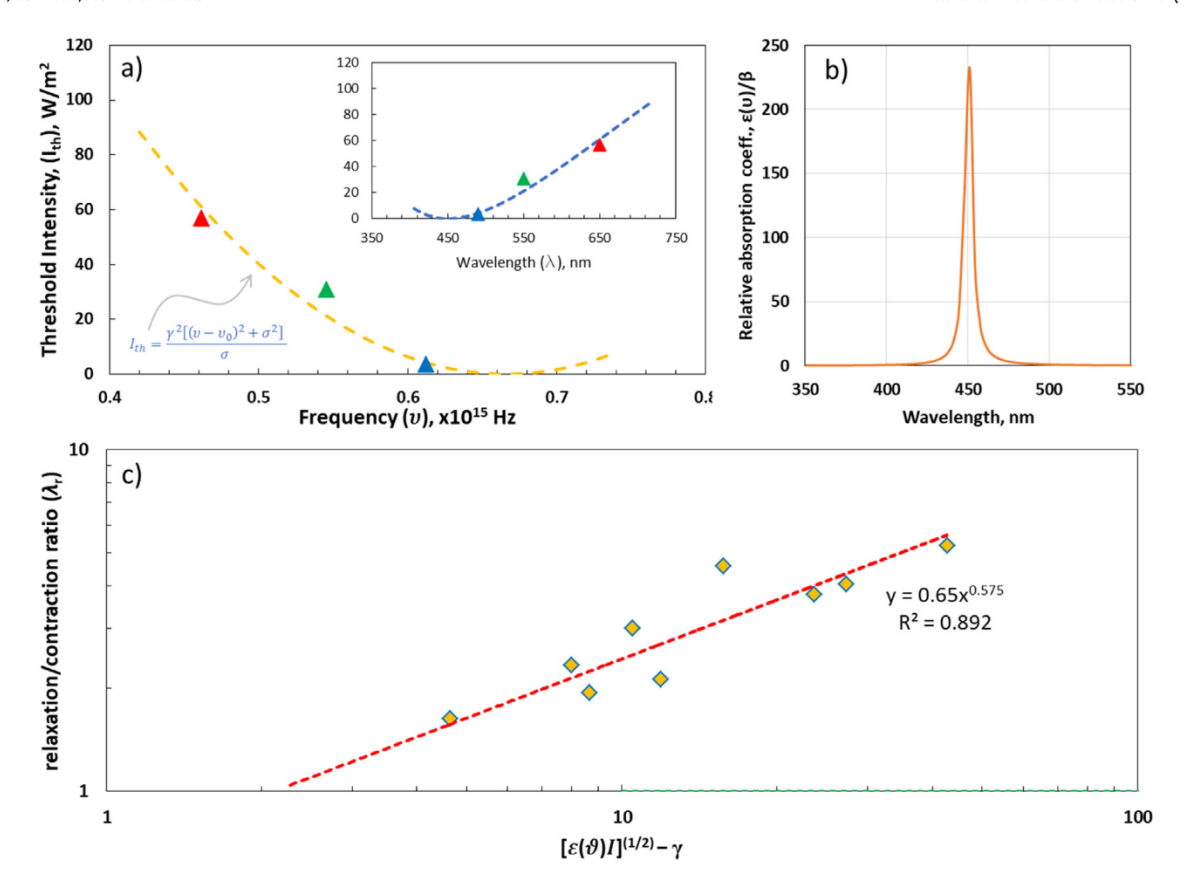


Fig. 7. (a) Photoreaction based model for threshold intensity. The red, green and blue markers show experimental data points and the orange dashed line is the fitted model for threshold intensity in frequency space. The inset presents the same model in wavelength domain. (b) Relative absorption coefficient, ε(ν)/β based on the proposed model. The model shows that the absorption peak for CV-1 cells and culture media is 450 nm, which is potentially the most damaging light for this particular cell line. (c) Correlation between photo-toxicity and light intensity. Relaxation/contraction ratio  $(λ_r)$  has a power relationship with illumination intensities above  $I = 57 \text{ W/m}^2$ .  $λ_r$  can be predicted by the fitted line (red dotted) with equation  $λ_r = α_2(rt - r_{th}t)^α$ . The markers represent data points from experiments with  $I \ge 57 \text{ W/m}^2$ .  $λ_r$  vs I curve is shown in Suppl. Fig. 8.. (For interpretation of the references to color in this figure legend, the reader is referred to the web version of this article.)

Long exposure experiments conducted on fibroblasts (CV-1) on laminin coated substrates verify similar safety limits for light intensities (Fig. 6). These results suggest that the threshold intensities are independent of the ECM the cells are adhered to. Overall, these results clearly demonstrate that if illumination intensity can be maintained below thresholds, energy dosage can be dramatically increased without inducing photo-toxicity. For instance, a dosage of  $\sim\!4500~\text{J/m}^2$  was sufficient to induce force relaxation (Fig. 5g-h) with 235 W/m²red light; whereas  $\sim\!400,000~\text{J/m}^2$  dosage ( $\sim\!100~\text{times higher}$ ) with threshold intensity red light (57 W/m², Fig. 4e-f) did not affect cell traction. This is a critical information for time lapse imaging, since lower intensities may compromise resolution. Now, the effect of low intensity can be compensated by longer exposure time for imaging.

#### 4. Discussion

It is well acknowledged that cells and tissues can be photosensitive [41]. Various cell functions has been used to measure photosensitivity, such as apoptosis and cell death [13,14,42], gene expressions [43,44], cell division [1,45], and subcellular signaling [46,47]. For example, Wäldchen et al. [13] found that 50% of COS-7 (monkey kidney fibroblast) cells die when exposed to 514 nm green light with intensity and dosage of 5 MW/m² and 1200 MJ/m² respectively. Threshold intensity (dosage) for apoptosis in COS-7 were found to be 0.2 (0.4), 2 (480) and 20 (4800) MW/m² (MJ/m²) for 405, 514 and 640 nm lights respectively. Wagner et al. [42] studied colony formation efficiency of glioblastoma cells and recommended light dosage of 1 and 2 MJ/m²

with 514 and 633 nm lights, for non-photo-toxic fluorescent imaging. Here, we exploited cell traction as a measure of their photosensitivity. We find that cells may relax their traction at intensities and dosages that are 5 orders of magnitude lower than those needed for apoptotic response (intensity 7.35 kW/m² and dosage 441 kJ/m² for green light, Fig. 1). The threshold intensities of light below which cells become insensitive to dosages depends on wavelengths.

Mechanism of photo-toxicity may vary with cell types, culture conditions and illumination protocols. Potential mechanisms may involve production of reactive oxygen species (ROS), a family of volatile chemicals e.g. superoxide anion  $(\mathrm{O}_2^-)$ , hydrogen peroxide  $(H_2O_2)$  and hydroxyl radical  $(HO^-)$  within the cells [45,48] or in the culture media [14,44]. A growing list of literature supports that visible light ( $\lambda = 380-700$  nm) is also responsible for formation of free radicals and ROS leading to oxidative stress related damages in cells and tissues [48-53]. ROS is known to regulate several signaling pathways affecting a variety of cellular processes, such as proliferation, metabolism, differentiation, and survival [54–56]. However, it is not clear how ROS affects cellular traction. Dixit and Cyr [45] showed that mitosis of BY-2 tobacco cells can be arrested by ROS produced by fluorescent lights above a threshold dosage of 7900 J/m<sup>2</sup> at 133 W/m<sup>2</sup> intensity with 460-500 nm light (0.5 s exposure every 30 s for a total 60 min). Their results suggest that cells can survive illumination for short duration. With continuous illumination, ROS accumulation leads to physiological damage. The rate of ROS production and mitotic arrest are correlated with energy dosage, as well as excitation light intensity.

In this study, we focused on visible light and discussed the influence of wavelengths between  $\lambda = 400-700$  nm on cell traction. In order to interpret the experimental observations, we consider a simplified but generalizable model to relate cell photorelaxation with light exposure. We propose that relaxation process proceeds in three steps: (1) light is absorbed by photosensitive agents within the cell. While the absorbed energy depends on the absorption spectra of the specific agents, the overall consequence is that the ratio of transmitted,  $I_t$ , to incident intensity,  $I_0$ , for a given frequency of light is provided by the Beer-Lambert law [57,58] as  $I_t(z) = I_0 e^{-\sum_i a_i m_i z}$ , where  $a_i$  are the absorption coefficients of the absorbers,  $m_i$  are their concentrations and z is the thickness of the cell along the light path. Here we assume that  $a_i$ ,  $m_i$  are uniform through the cell thickness. The absorbed intensity,  $I_a$  is then given by,  $I_a = I_0 (1 - e^{-\varepsilon})$ , where  $\varepsilon(\vartheta) = \sum_i a_i m_i z$  is dimensionless, but depends on the frequency of light. We expect that most of the light is transmitted through the cell and hence  $\varepsilon(\vartheta) \ll 1$ . Applying Taylor series expansion and neglecting higher order terms, we have,  $I_a = I_0 (1 - e^{-\varepsilon}) \approx I_0 \varepsilon (\vartheta)$ , and  $\varepsilon (\vartheta) = I_a/I_0$ . (2) The photo-activated agents produce chemicals, C, with a rate r (per unit time within the volume of cell-media exposed to light). Thus, r depends on the rate of absorbed energy,  $\varepsilon(\vartheta)I$ , where I is the intensity of the incident light. (3) Cells sequester or neutralize the chemical products at a fixed rate,  $r_{th}$ . If r is low due to low light absorption, cell traction remains unperturbed by light. If  $r > r_{th}$ , cells respond by relaxing with a rate  $d\lambda_r/dt$ . Note that, experimentally we measured  $\lambda_r$  at time t = 60 s, when cells were exposed to light continuously for 60 s. We propose the following

$$\varepsilon(v) = \beta \frac{\sigma}{(v - v_0)^2 + \sigma^2}$$
 (1)

$$r = \alpha_1 [\varepsilon (\vartheta) I]^{1/2} \tag{2}$$

$$\lambda_r = \begin{cases} 0, r \le r_{th} \\ \alpha_2 (rt - r_{th}t)^{\alpha} = \alpha_2 t^{\alpha} (r - r_{th})^{\alpha}, r > r_{th} \end{cases}$$
 (3)

To simulate the frequency dependence of absorption of incident light, we chose a Lorentzian model [59] for  $\varepsilon(\vartheta)$  in Eq. (1). Here,  $\vartheta_0$  is the central frequency,  $\sigma$  is the full width at half maximum;  $\alpha$ ,  $\alpha_1$ ,  $\alpha_2$  and  $\beta$  are constants. The exponent  $\frac{1}{2}$  in Eq. (2) is motivated by earlier studies on photo reactions [60–62]. Eq. (3) is based on a power law dependence between photorelaxation and reaction rate. In order to cause photorelaxation, it is conceivable that the reaction products C diffuse from the site of production to the sites within the cell where traction is generated. Due to this potential diffusion type transport mechanism, we expect  $\alpha=1/2$  in  $\lambda_r \sim t^\alpha$ , for a given I and  $\upsilon$ . We will verify the hypothesis of  $\alpha=1/2$  in the following.

In Eq. (3), at threshold light,  $I_{th}$ ,  $\lambda_r = 0$ , and  $r = r_{th}$ , which together with Eqs. (1) and (2) give  $I_{th}$ :

$$I_{th} = \frac{\gamma^2 \left[ (\upsilon - \upsilon_0)^2 + \sigma^2 \right]}{\sigma} \tag{4}$$

Here  $\gamma=\frac{r_{th}}{\alpha_1\beta^2}$ . We have experimental measures of  $I_{th}$  for three corresponding values of  $\upsilon$ . By best fitting  $I_{th}$  versus  $\upsilon$  to Eq. (4), we obtain  $\gamma=2.4\sqrt{J}/m$ ,  $\upsilon_0=0.666$  PHz, and  $\sigma=0.004$  PHz (Fig. 7a). Using  $\upsilon_0$  and  $\sigma$ , we plot the spectral density function,  $\varepsilon\left(\upsilon\right)/\beta$  (Fig. 7b) which suggests highest photosensitivity at wavelength of 450 nm. However, sensitivity decreases sharply with change in wavelength.

Eq. (3) can be written as:  $\lambda_r = \alpha_2 t^{\alpha} (r - r_{th})^{\alpha} = \alpha_1 \alpha_2 t^{\alpha} \sqrt{\beta}$  [ $(\frac{l\sigma}{(\nu - \nu_0)^2 + \sigma^2})^{\frac{1}{2}} - \gamma$ ],  $r > r_{th}$ . We have experimental values of  $\lambda_r (t = 60)$  s and the corresponding light intensity I and frequency  $\vartheta$ . These, together with known values of  $\gamma$ ,  $\vartheta_0$ ,  $\sigma$ , allow us to

plot  $\lambda_r$  versus  $[(\frac{I\sigma}{(\nu-\nu_0)^2+\sigma^2})^{\frac{1}{2}}-\gamma]$  in log-log scale (Fig. 7c). The slope gives the exponent  $\alpha=0.575$ , close to  $\frac{1}{2}$  as speculated. Thus Eq. (3) with  $\alpha=1/2$  can be used to predict possible photorelaxation for wavelengths between 400 and 700 nm. While the precise mechanisms and fluxes should be examined in detail, our purpose here was to present an easy-to-use model that can enable a practitioner to estimate safe levels of illumination for particular experimental conditions.

Threshold intensity reported in this paper is based on relaxation of cellular traction. As discussed previously, monitoring other functional responses from cells or tissues may reveal different safe intensities. Also, despite covering the effect of most widely used excitation wavelength regions - blue, green and red ( $\lambda \sim 480 - 650$  nm) on cells, photosensitivity due to shorter and longer wavelengths remain to be seen. We do anticipate greater sensitivity to shorter wavelengths [63] as electronic transitions can be excited and molecular transitions at longer wavelengths [64], potentially offering a route to modulating relaxation with spectrally-selective illumination. However, based on our current knowledge, cell traction relaxation appears to be the most sensitive functional output to photosensitivity. For instance, previously reported safe threshold intensity for blue light was found to be 200 kW/m<sup>2</sup> and 133 W/m<sup>2</sup> based on cell death [13] and mitosis arrest [45] respectively. Whereas, our results suggest a significantly lower safe threshold of 3.5 W/m<sup>2</sup> for blue light; establishing that cell traction relaxation is a very sensitive functional output. Hence, the study offers an approach/methodology for determining safe intensity of visible light for live cell/tissue microscopy based on cell traction. The study may also provide guidelines to explore the use of light for cancer therapeutics where photo toxicity of cancer cells and tumors might be exploited.

#### 5. Conclusion

Light excitation has long been used to excite and observe fluorescence in living cells, but the effect of light on cell functions still remains to be fully described. Currently, there exists no definitive quantitative means to assess cell photo-response in real time. Furthermore, an exposure limit for mitigating photo-induced cell changes has not yet been established. Here, we search for a light intensity that has minimal effect on cells and yet that is sufficient for time-lapse fluorescent imaging. We exploit photosensitivity of fibroblasts to establish the threshold. Fibroblasts relax their contractility when exposed to light, and their photorelaxation depends on light intensity, wavelength and dosage (exposure time). We find that monkey (kidney fibroblast, CV-1), human (colon normal fibroblast, CCD-112 CoN) and mouse (fibroblasts, NIH/3T3) cells are all photo-sensitive, independent of their ECM (e.g., fibronectin, laminin and collagen) and whether they are on 2D or 3D culture platforms. We report that phototoxicity can be avoided by application of lights below certain intensities that we refer to as safe thresholds. We also establish 57, 31 and 3.5 W/m<sup>2</sup> as threshold intensities for red, green and blue lights, respectively. To our knowledge, these intensities are the lowest reported safe thresholds and thus cellular traction relaxation is the most sensitive functional readout for photosensitivity. Most notably, we discovered that cell contractility becomes insensitive to light dosage (and exposure time) below threshold intensities, although higher dosage results in more relaxation for lights above threshold. This finding is particularly significant for long duration time-lapse microscopy and imaging techniques that require long exposures. Moreover, these threshold intensities provide sufficient resolution for fluorescence imaging using standard cameras. We finally present a photo-reaction based

model of photo-toxicity to predict threshold intensity for different light wavelengths in the visible spectra. We suggest adopting lights with intensities below the dose-independent thresholds, predicted by the model, for fluorescence imaging of living cells in 2D and 3D culture.

## **CRediT authorship contribution statement**

M.A. Bashar Emon: Conceived and designed the experiments, Performed the experiments, Analyzed the data, Manuscript preparation. Samantha Knoll: Conceived and designed the experiments, Performed the experiments, Analyzed the data, Manuscript preparation. Umnia Doha: Performed the experiments, Analyzed the data. Lauren Ladehoff: Performed the experiments, Analyzed the data. Luke Lalonde: Performed the experiments, Analyzed the data. Danielle Baietto: Performed the experiments. Mayandi Sivaguru: Performed the experiments. M. Taher A. Saif: Conceived and designed the experiments, Analyzed the data, Manuscript preparation.

#### **Declaration of competing interest**

The authors declare that they have no known competing financial interests or personal relationships that could have appeared to influence the work reported in this paper.

#### **Data availability**

All data generated or analyzed during this study are included in this published article (and its Supplementary Information files).

#### Acknowledgments

Research reported in this publication was supported by the National Institute of Biomedical Imaging and Bioengineering of the National Institutes of Health, United States under Award Number

T32EB019944, NSF CMMI, United States 1742908, NSF ECCS, United States 1934991 and Illinois Cancer Center seed grant. The content is solely the responsibility of the authors and does not necessarily represent the official views of the National Institutes of Health. All authors have read and approved the final manuscript.

# Appendix A. Supplementary data

Supplementary material related to this article can be found online at https://doi.org/10.1016/j.eml.2021.101249.

#### References

- A. Khodjakov, C.L. Rieder, Imaging the division process in living tissue culture cells, Methods 38 (2006) 2–16, https://doi.org/10.1016/j.ymeth. 2005.07.007.
- [2] J. Xiao, Single-molecule imaging in live cells, in: Handb. Single-Molecule Biophys, Springer US, New York, NY, 2009, pp. 43–93, https://doi.org/10. 1007/978-0-387-76497-9\_3.
- [3] M.M. Frigault, J. Lacoste, J.L. Swift, C.M. Brown, Live-cell microscopy -Tips and tools, J. Cell Sci. 122 (2009) 753–767, https://doi.org/10.1242/ jcs.033837.
- [4] R.F. Furchgott, The pharmacology of vascular smooth muscle, Pharmacol. Rev. 7 (1955).
- [5] S.J. Ehrreich, R.F. Furchgott, Relaxation of mammalian smooth muscles by visible and ultraviolet radiation, Nature 218 (1968) 682–684.
- 6] S.G. Knoll, Exposure To Fluorescent Excitation Light Induces Dose-Dependent, Irreversible Force Relaxation in Living Fibroblast Cells, University of Illinois, Urbana-Champaign, 2016, https://www.ideals. illinois.edu/bitstream/handle/2142/90923/KNOLL-DISSERTATION-2016.pdf?sequence=1&isAllowed=y.

- [7] H. Yawo, T. Asano, S. Sakai, T. Ishizuka, Optogenetic manipulation of neural and non-neural functions, Dev. Growth Differ. 55 (2013) 474–490, https://doi.org/10.1111/dgd.12053.
- [8] S. Cox, E. Rosten, J. Monypenny, T. Jovanovic-Talisman, D.T. Burnette, J. Lippincott-Schwartz, G.E. Jones, R. Heintzmann, Bayesian localization microscopy reveals nanoscale podosome dynamics, Nat. Methods 9 (2012) 195–200, https://doi.org/10.1038/nmeth.1812.
- [9] R. Henriques, C. Griffiths, E.H. Rego, M.M. Mhlanga, PALM And STORM: Unlocking live-cell super-resolution, Biopolymers 95 (2011) 322–331, https://doi.org/10.1002/bip.21586.
- [10] F. St-Pierre, J.D. Marshall, Y. Yang, Y. Gong, M.J. Schnitzer, M.Z. Lin, High-fidelity optical reporting of neuronal electrical activity with an ultrafast fluorescent voltage sensor, Nat. Neurosci. 17 (2014) 884–889, https://doi.org/10.1038/nn.3709.
- [11] Z. Liu, L.D. Lavis, E. Betzig, Imaging live-cell dynamics and structure at the single-molecule level, Mol. Cell. 58 (2015) 644–659, https://doi.org/10. 1016/j.molcel.2015.02.033.
- [12] N. Ji, H. Shroff, H. Zhong, E. Betzig, Advances in the speed and resolution of light microscopy, Curr. Opin. Neurobiol. 18 (2008) 605–616, https: //doi.org/10.1016/j.conb.2009.03.009.
- [13] S. Wäldchen, J. Lehmann, T. Klein, S. van de Linde, M. Sauer, Light-induced cell damage in live-cell super-resolution microscopy, Sci. Rep. 5 (2015) 15348, https://doi.org/10.1038/srep15348.
- [14] J.H. Stockley, K. Evans, M. Matthey, K. Volbracht, S. Agathou, J. Mukanowa, J. Burrone, R.T. Káradóttir, Surpassing light-induced cell damage in vitro with novel cell culture media, Sci. Rep. 7 (2017) https://doi.org/10.1038/ s41598-017-00829-x.
- [15] R.S. Stern, N. Laird, J. Melski, J.A. Parrish, T.B. Fitzpatrick, H.L. Bleich, Cutaneous squamous-cell carcinoma in patients treated with PUVA, N. Engl. J. Med. 310 (1984) 1156–1161, https://doi.org/10.1056/NEJM198405033101805.
- [16] D.H. Kessel, M. Price, J.J. Reiners Jr., ATG7 deficiency suppresses apoptosis and cell death induced by lysosomal photodamage, Autophagy 8 (2012) 1333–1341, https://doi.org/10.4161/auto.20792.
- [17] T. Lindl, R. Steubing, Atlas of Living Cell Cultures, Wiley-Blackwell, 2013.
- [18] Artifacts of light, Nat. Methods 10 (2013) 1135, https://doi.org/10.1038/ nmeth.2760.
- [19] J.Y. Tinevez, J. Dragavon, L. Baba-Aissa, P. Roux, E. Perret, A. Canivet, V. Galy, S. Shorte, A quantitative method for measuring phototoxicity of a live cell imaging microscope, in: Methods Enzymol., Academic Press Inc., 2012, pp. 291–309, https://doi.org/10.1016/B978-0-12-391856-7.00039-1.
- [20] A. de With, K.O. Greulich, Wavelength dependence of laser-induced DNA damage in lymphocytes observed by single-cell gel electrophoresis, J. Photochem. Photobiol. B Biol. 30 (1995) 71-76, https://doi.org/10.1016/1011-1344(95)07151-Q.
- [21] J.R. Lange, B. Fabry, Cell and tissue mechanics in cell migration, Exp. Cell Res. 319 (2013) 2418–2423, https://doi.org/10.1016/j.yexcr.2013.04.023.
- [22] E.P. Canović, A.J. Zollinger, S.N. Tam, M.L. Smith, D. Stamenović, Tensional homeostasis in endothelial cells is a multicellular phenomenon, Am. J. Physiol. Physiol. 311 (2016) C528-C535, https://doi.org/10.1152/ajpcell. 00037 2016
- [23] E. Bellas, C.S. Chen, Forms, forces, and stem cell fate, Curr. Opin. Cell Biol. 31 (2014) 92–97, https://doi.org/10.1016/j.ceb.2014.09.006.
- [24] H. Taylor-Weiner, N. Ravi, A.J. Engler, Traction forces mediated by integrin signaling are necessary for definitive endoderm specification, J. Cell Sci. 128 (2015) 1961–1968, https://doi.org/10.1242/jcs.166157.
- [25] B. Li, J.H.-C. Wang, Fibroblasts and myofibroblasts in wound healing: force generation and measurement, J. Tissue Viability 20 (2011) 108–120, https://doi.org/10.1016/j.jtv.2009.11.004.
- [26] J.H.-C. Wang, B. Li, Application of Cell Traction Force Microscopy for Cell Biology Research, Humana Press, 2009, pp. 301–313, https://doi.org/10. 1007/978-1-60761-376-3\_17.
- [27] B. Emon, J. Bauer, Y. Jain, B. Jung, T. Saif, Biophysics of tumor microenvironment and cancer metastasis A mini review, Comput. Struct. Biotechnol. J. 16 (2018) 279–287, https://doi.org/10.1016/j.csbj.2018.07.003.
- [28] J. Bauer, J.J. Staudacher, G. Mancinelli, N. Krett, E. Bashar, P. Grippo, M.T.A. Saif, B. Jung, Abstract 177: Increased stiffness of the tumor microenvironment in colon cancer leads to an increase in activin and metastatic potential, in: Tumor Biol., American Association for Cancer Research, 2018, p. 177, https://doi.org/10.1158/1538-7445.AM2018-177.
- [29] J.-K. Chang, M.A.B. Emon, C.-S. Li, Q. Yang, H.-P. Chang, Z. Yang, C.-I. Wu, M.T. Saif, J.A. Rogers, Cytotoxicity and in vitro degradation kinetics of foundry-compatible semiconductor nanomembranes and electronic microcomponents, ACS Nano. 12 (2018) 9721–9732, https://doi.org/10.1021/acsnano.8b04513.
- [30] S.G. Knoll, W.W. Ahmed, T.A. Saif, Contractile dynamics change before morphological cues during fluorescence illumination, Sci. Rep. 5 (2016) 18513, https://doi.org/10.1038/srep18513.
- [31] Y. Brill-Karniely, N. Nisenholz, K. Rajendran, Q. Dang, R. Krishnan, A. Zemel, Dynamics of cell area and force during spreading, Biophys. J. 107 (2014) L37–L40, https://doi.org/10.1016/j.bpj.2014.10.049.

- [32] N. Nisenholz, K. Rajendran, Q. Dang, H. Chen, R. Kemkemer, R. Krishnan, A. Zemel, Active mechanics and dynamics of cell spreading on elastic substrates, Soft Matter. 10 (2014) 7234, https://doi.org/10.1039/C4SM00780H.
- [33] S.G. Knoll, M.T.A. Saif, Light induced, localized, and abrupt force relaxations in fibroblast cells on soft substrates, Extrem. Mech. Lett. 8 (2016) 257–265, https://doi.org/10.1016/J.EML.2016.03.009.
- [34] S.G. Knoll, M.Y. Ali, M.T.A. Saif, A novel method for localizing reporter fluorescent beads near the cell culture surface for traction force microscopy, J. Vis. Exp. (2014) 51873, https://doi.org/10.3791/51873.
- [35] J.R. Tse, A.J. Engler, Preparation of hydrogel substrates with tunable mechanical properties, Curr. Protoc. Cell Biol. 47 (2010) 10.16.1-10.16.16. https://doi.org/10.1002/0471143030.cb1016s47.
- [36] Corning Incorporated, Certificate of Analysis for Corning Collagen I High concentration (HC), Rat Tail, 2020, https://certs-ecatalog.corning.com/lifesciences/certs/354249\_9343002.pdf. (Accessed 5 July 2020).
- [37] T. Iskratsch, H. Wolfenson, M.P. Sheetz, Appreciating force and shape the rise of mechanotransduction in cell biology, Nat. Rev. Mol. Cell Biol. 15 (2014) 825–833, https://doi.org/10.1038/nrm3903.
- [38] P. Roca-Cusachs, T. Iskratsch, M.P. Sheetz, Finding the weakest link exploring integrin-mediated mechanical molecular pathways, J. Cell Sci. 125 (2012) 3025–3038, https://doi.org/10.1242/jcs.095794.
- [39] C.A. Reinhart-King, M. Dembo, D.A. Hammer, The dynamics and mechanics of endothelial cell spreading, Biophys. J. 89 (2005) 676–689, https://doi. org/10.1529/biophysj.104.054320.
- [40] A. Saez, A. Buguin, P. Silberzan, B. Ladoux, Is the mechanical activity of epithelial cells controlled by deformations or forces? Biophys. J. 89 (2005) L52–L54, https://doi.org/10.1529/BIOPHYSJ.105.071217.
- [41] P.P. Laissue, R.A. Alghamdi, P. Tomancak, E.G. Reynaud, H. Shroff, Assessing phototoxicity in live fluorescence imaging, Nat. Methods 14 (2017) 657–661, https://doi.org/10.1038/nmeth.4344.
- [42] M. Wagner, P. Weber, T. Bruns, W.S.L. Strauss, R. Wittig, H. Schneck-enburger, Light dose is a limiting factor to maintain cell viability in fluorescence microscopy and single molecule detection, Int. J. Mol. Sci. 11 (2010) 956–966, https://doi.org/10.3390/ijms11030956.
- [43] K.M. Tyssowski, J.M. Gray, Blue light increases neuronal activity-regulated gene expression in the absence of optogenetic proteins, ENeuro. 6 (2019) https://doi.org/10.1523/ENEURO.0085-19.2019.
- [44] C.G. Duke, K.E. Savell, J.J. Tuscher, R.A. Phillips, J.J. Day, Blue light-induced gene expression alterations in cultured neurons are the result of phototoxic interactions with neuronal culture media, ENeuro. 7 (2020) 386–405, https://doi.org/10.1523/ENEURO.0386-19.2019.
- [45] R. Dixit, R. Cyr, Cell damage and reactive oxygen species production induced by fluorescence microscopy: Effect on mitosis and guidelines for non-invasive fluorescence microscopy, Plant J. 36 (2003) 280–290, https://doi.org/10.1046/j.1365-313X.2003.01868.x.
- [46] D. Tischer, O.D. Weiner, Illuminating cell signalling with optogenetic tools, Nat. Rev. Mol. Cell Biol. 15 (2014) 551–558, https://doi.org/10.1038/ nrm3837.
- [47] W.K. Ajith Karunarathne, P.R. O'Neill, N. Gautam, Subcellular optogenetics -Controlling signaling and single-cell behavior, J. Cell Sci. 128 (2015) 15–25, https://doi.org/10.1242/jcs.154435.
- [48] L.-D. Arthaut, N. Jourdan, A. Mteyrek, M. Procopio, M. El-Esawi, A. d'Harlingue, P.-E. Bouchet, J. Witczak, T. Ritz, A. Klarsfeld, S. Birman, R.J. Usselman, U. Hoecker, C.F. Martino, M. Ahmad, Blue-light induced accumulation of reactive oxygen species is a consequence of the drosophila cryptochrome photocycle, PLoS One. 12 (2017) e0171836, https://doi.org/10.1371/journal.pone.0171836.

- [49] L. Zastrow, N. Groth, F. Klein, D. Kockott, J. Lademann, R. Renneberg, L. Ferrero, The missing link - Light-induced (280-1,600 nm) free radical formation in human skin, Skin Pharmacol. Physiol. 22 (2009) 31–44, https: //doi.org/10.1159/000188083.
- [50] L. Zastrow, N. Groth, F. Klein, D. Kockott, J. Lademann, L. Ferrero, UV, sichtbares Licht, Infrarot: Welche Wellenlängen produzieren oxidativen Stress in menschlicher Haut? Hautarzt. 60 (2009) 310–317, https://doi.org/10.1007/s00105-008-1628-6.
- [51] C. Kielbassa, L. Roza, B. Epe, Wavelength dependence of oxidative DNA damage induced by UV and visible light, Carcinogenesis 18 (1997) 811–816, https://doi.org/10.1093/carcin/18.4.811.
- [52] T. Mann, K. Eggers, F. Rippke, M. Tesch, A. Buerger, M.E. Darvin, S. Schanzer, M.C. Meinke, J. Lademann, L. Kolbe, High-energy visible light at ambient doses and intensities induces oxidative stress of skin—Protective effects of the antioxidant and Nrf2 inducer Licochalcone A in vitro and in vivo, Photodermatol. Photoimmunol. Photomed. 36 (2020) 135–144, https://doi.org/10.1111/phpp.12523.
- [53] C.S. Uyguner, M. Bekbolet, Evaluation of humic acid photocatalytic degradation by UV-vis and fluorescence spectroscopy, in: Catal. Today, Elsevier, 2005, pp. 267–274, https://doi.org/10.1016/j.cattod.2005.03.011.
- [54] Z. Liao, D. Chua, N.S. Tan, Reactive oxygen species: A volatile driver of field cancerization and metastasis, Mol. Cancer. 18 (2019) 65, https: //doi.org/10.1186/s12943-019-0961-y.
- [55] M.P. Murphy, A. Holmgren, N.G. Larsson, B. Halliwell, C.J. Chang, B. Kalyanaraman, S.G. Rhee, P.J. Thornalley, L. Partridge, D. Gems, T. Nyström, V. Belousov, P.T. Schumacker, C.C. Winterbourn, Unraveling the biological roles of reactive oxygen species, Cell Metab. 13 (2011) 361–366, https://doi.org/10.1016/j.cmet.2011.03.010.
- [56] P.D. Ray, B.W. Huang, Y. Tsuji, Reactive oxygen species (ROS) homeostasis and redox regulation in cellular signaling, Cell. Signal. 24 (2012) 981–990, https://doi.org/10.1016/j.cellsig.2012.01.008.
- [57] D.F. Swinehart, The Beer-Lambert law, J. Chem. Educ. 39 (1962) 333–335, https://doi.org/10.1021/ed039p333.
- [58] G. Wypych, Handbook of UV Degradation and Stabilization, second ed., Elsevier Inc., 2015, https://doi.org/10.1016/C2014-0-01351-2.
- [59] A.J. Brown, Spectral curve fitting for automatic hyperspectral data analysis, IEEE Trans. Geosci. Remote Sens. 44 (2014) 1601–1607, https://doi.org/10. 1109/TGRS.2006.870435.
- [60] Y. Nosaka, A.Y. Nosaka, Langmuir-hinshelwood and light-intensity dependence analyses of photocatalytic oxidation rates by two-dimensional-ladder kinetic simulation, J. Phys. Chem. C. 122 (2018) 28748–28756, https://doi.org/10.1021/acs.jpcc.8b09421.
- [61] J.Z. Bloh, A holistic approach to model the kinetics of photocatalytic reactions, Front. Chem. 7 (2019) 128, https://doi.org/10.3389/fchem.2019. 00138
- [62] J.S. Miller, L. Nowicki, S. Ledakowicz, Kinetics of tetrachloroethene photochlorination in a homogeneous system, Chem. Eng. Technol. 16 (1993) 429-432, https://doi.org/10.1002/ceat.270160612.
- [63] S. Soltani, A. Ojaghi, F.E. Robles, Deep UV dispersion and absorption spectroscopy of biomolecules, Biomed. Opt. Express. 10 (2019) 487, https: //doi.org/10.1364/boe.10.000487.
- [64] M.J. Baker, J. Trevisan, P. Bassan, R. Bhargava, H.J. Butler, K.M. Dorling, P.R. Fielden, S.W. Fogarty, N.J. Fullwood, K.A. Heys, C. Hughes, P. Lasch, P.L. Martin-Hirsch, B. Obinaju, G.D. Sockalingum, J. Sulé-Suso, R.J. Strong, M.J. Walsh, B.R. Wood, P. Gardner, F.L. Martin, Using Fourier transform IR spectroscopy to analyze biological materials, Nat. Protoc. 9 (2014) 1771-1791, https://doi.org/10.1038/nprot.2014.110.